Sensors and Materials, Vol. 12, No. 2 (2000) 069–077
MYU Tokyo

S & M 0397

Non-Destructive Evaluation System Based on High-T_c Superconducting Quantum Interference Device Sensors

George Kallias[1], Eamonn Devlin[1], Christos Christides[1,2] and Dimitris Niarchos[1]

[1]Institute of Materials Science, NCSR "DEMOKRITOS," 153 10 Athens, Greece
[2]Department of Engineering Sciences, School of Engineering, University of Patras, 26110 Patras, Greece

(Received December 24, 1999; accepted April 17, 2000)

Key words: High-T_c SQUIDs, non-destructive evaluation, magnetic field mapping

We present magnetic field mapping measurements performed with commercial high-T_c superconducting quantum interference device (SQUID) sensors. Our aim was to make an initial assessment of the capabilities of our commercial high-T_c sensors (and of the entire system incorporating them) under zero applied magnetic field. This allowed us to measure signals of the order of 0.5 nT. In all cases the experimental field map was consistent with the theoretically expected images. In measurements with two samples, the relative orientation and center-to-center separation of the samples could be easily deduced from the field map. Some initial tests on surface flaw detection of unglazed ceramic tiles under an externally applied magnetic field are also discussed.

1. Introduction

The use of low critical temperature (T_c) superconducting quantum interference device (SQUID) sensors in non-destructive evaluation (NDE) was introduced some ten years ago with the pioneering work of Weinstock Nisenoff[1,2] as another form of magnetic anomaly detection, and they were demonstrated in the detection of flaws in steel pipes and plates. In 1982, Donaldson's University of Strathclyde group used SQUID magnetic gradiometry to detect surface cracks in ferromagnetic steel plates.[3] In recent years, Wikswo and coworkers at Vanderbilt University have applied SQUID magnetometry and gradiometry to a variety of problems in biomagnetism and NDE[4–8] using MicroSQUID, a system based on low-T_c sensors that can have a minimum sample-to-sensor distance of 1.5 mm.[9]

A simple description of a SQUID is that of a black box that converts magnetic flux into

voltage with unparalleled sensitivity. Their sensitivity allows them to function with much smaller pickup coils than other sensors at a given field sensitivity. In addition to their very high magnetic flux sensitivity, their high linearity, wide bandwidth (from dc to 50 kHz) and broad dynamic range (130 dB) renders them suitable for a variety of applications (biomagnetism, geophysics) and, of course, NDE applications. Their ability to operate down to zero frequency allows them to detect deeper flaws (*e.g.*, originating from rivet holes) than traditional eddy current sensors, while their broad dynamic range preserves their high sensitivity in strong dc or noise fields.

For high-T_c SQUIDs, the tremendous improvement in sensor and coil fabrication has allowed their use in real applications. Their operation in actual world environments has been addressed in a number of published reports[10–12] and their use in gradiometer configurations resulted in system noise levels of 180 fT/Hz$^{1/2}$ at 77 K in unshielded laboratory environments.[13] For optimum performance, the use of SQUID applications in unshielded environments requires in general an axial gradiometer with large baseline and a high balance. Electronic gradiometers based on several magnetometers are commonly used. A SQUID vector reference consisting of three magnetometers oriented in x, y and z directions with the sensing SQUID being z-oriented was recently implemented for operation in unshielded environments[14] with satisfactory results.

NDE SQUID magnetometry has been applied to flaw characterization, analysis of magnetic properties of materials and corrosion studies (see ref. (15) and references therein). The SQUID measures the magnetic flux at multiple locations in the vicinity of the test object, giving a map or image of the magnetic field. This enables the user to detect, locate and evaluate discontinuities, defects or other imperfections. The magnetic field sources can be intrinsic in the test object (corrosion, magnetized samples) or can be provided by an external source (injected current or applied magnetic field).

Wikswo[15] has provided a market oriented overview of SQUIDs for biomagnetism and NDE. High-T_c SQUIDs can be used in practical applications because they have less stringent cooling requirements than low-T_c SQUIDs, a factor that allows portability of the system. In addition, liquid nitrogen is considerably cheaper, more readily available and easier to transport than liquid helium. For these reasons there is considerable effort in establishing the use of high-T_c SQUIDs in a variety of NDE applications.[16–21] Although NDE is useful in many fields, two of the most interesting are ageing aircraft and ageing and crack development in chemical and nuclear reactor pressure vessels.[22]

Our aim in this work is to make an initial assessment of the capabilities of our commercial high-T_c sensors (and of the entire system incorporating them) under zero applied magnetic field. Surface flaw detection of ceramic materials under an externally applied magnetic field is also discussed.

2. Experimental Setup and Description of Measurements

2.1 *Experimental setup*

The system consists of three high-T_c SQUID sensors (offset grain boundary type, Conductus Inc., with a pickup coil area of 3×3 mm^2) placed at the corners of an equilateral triangle with a side of 21.5 mm. In this way two electronic planar gradiometers are formed.

The SQUID sensors are hermetically sealed in a button-shaped glass-epoxy (G-10) package containing an integral heater that can heat the SQUIDs in case of flux trapping. All three SQUIDs are placed on the same probe which is housed in a fiberglass liquid nitrogen dewar. The sensor-to-sample distance is variable and can be as small as 5–6 mm, but in this case the liquid nitrogen consumption is dramatically increased. The probe and the dewar were purchased from Conductus Inc.

The SQUIDs were operated using a flux modulation technique (flux-locked loop) as a null detector of magnetic flux. The individual SQUID field-to-flux coefficients are 8.5, 8.5 and 8.3 nT/Φ_0, while the field noise was tabulated to be 89, 71 and 216 $fT/\sqrt{Hz}$, respectively. The SQUID controller also allowed reduction of the low-frequency noise by injecting a DC offset current into the modulation coil and thus nulling the DC output of the sensor. During the measurements we used a low-pass filter at 5 Hz.

The dewar with the sensors is surrounded by a cylindrical double-layer mu-metal shield (Kepston Q-Fab) with layers 1 mm thick and an air gap of 2 cm between the two layers. Without the mu-metal shield severe noise problems were encountered and the SQUIDs were unable to operate. A schematic overview of the NDE system is shown in Fig. 1.

A low-magnetic field xy scanning stage (Parker Motors) with 26 μm resolution, permits the displacement of the samples in two orthogonal directions. The stage is placed outside the mu-metal shield to avoid any background signals, even though its remanent field is 1/50th that of the earth's field at a distance of 17 mm above the stage. The

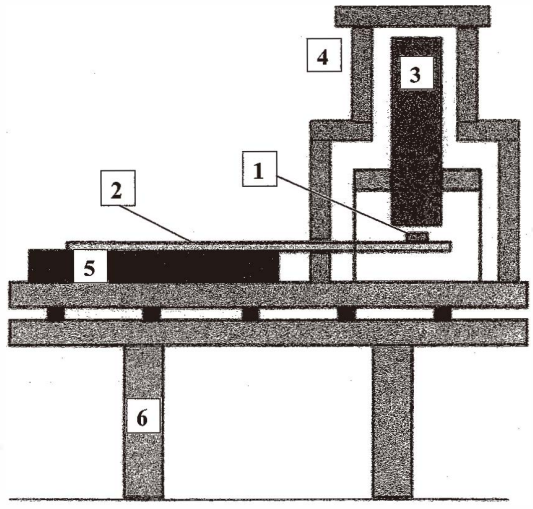

Fig. 1. A schematic presentation of the SQUID sensor-based NDE system. The sample [1] is placed on the plexiglass arm [2] and can move underneath the sensors, at variable distances, that are housed in a liquid nitrogen dewar [3] inside the double-layer mu-metal shield [4]. The sample is moved with the xy stage [5] placed outside the shielded enclosure. The marble table [6] consists of two surfaces separated by an anti-vibration material.

mechanical stability of the SQUID sensors is extremely important, particularly the isolation of low frequency vibrations, when operating the readout electronics in the most sensitive range.[23] To prevent such problems, the entire system was placed on a two-layer marble table with vibration-isolating rubber spacers between the layers.

2.2 *Description of measurements*

In a typical NDE experiment under zero applied magnetic field, the sample is moved underneath the SQUID sensors by means of a long plexiglass translation arm which penetrates the shield through an opening at one side. The other end of the plexiglass arm is firmly mounted on the scanning stage. A low-friction sample platform support within a side extension of the shield is used to prevent any undesirable vibrations caused by the movement of the plexiglass arm. The sample can be moved horizontally 300 mm × 300 mm (usually a 135 mm × 135 mm mesh was covered with 3 mm steps in both directions) by a pair of stepper motors (S-6, Parker Motors), computer controlled by an AT 6400 card using factory included software. The SQUIDs were heated and tuned before each scan to achieve optimum performance. The tuning parameters were always close to the calibration values. The outputs of the SQUIDs are sampled at each position, allowing a time interval of 250 ms for the SQUIDs to settle before each measurement. The scanning direction was always along the y-axis.

We measured the B_z component of the magnetic field of magnetized samples with the moment horizontally (x-y) and perpendicularly (z) oriented to assess the performance of the sensors under zero applied magnetic field. The first two samples were pieces of a common magnetic card with dimensions of 3 mm × 4 mm (sample I) and 3 mm × 5 mm (sample II). The magnetic field on the surface of the pieces was around 30 Gauss. The third sample was a pin 5 mm long with a diameter of 1 mm, magnetized along its axis (sample III). The magnetic field on the tip of the pin was 10 Gauss. Measurements of unglazed ceramic tiles were also performed under an external magnetic field produced by a system of compensating coils that were specially designed to null the field at the SQUIDs. To prevent undesirable fluctuations from the power supply and ensure stability of the current, the coils were powered by a gel cell battery. Before scanning, the samples were decorated with a paste of superparamagnetic particles (40% MAG/DVB, Seradyn Inc.). Then the paste was wiped from the surface of the sample with a piece of paper, remaining only inside the flaws.

3. Results

Initially, we measured the field produced by the pieces of magnetic card. First we measured sample I with its moment along the x-axis. Next we measured the same sample with its moment along the y-axis. This was done to identify any difference between these two cases, i.e., scanning directions parallel and perpendicular to the moment. Experimentally the two orientations of the moment were found to be indistinguishable, except of course for the finding that the observed dipole field was along the x- and y-axis each time. Here it is worth noting that a SQUID sensor measures the magnetic flux resulting from the component of the magnetic field that is normal to its surface and that for a magnetic field in the z+ (z–) direction, the SQUID's readout voltage is positive (negative). Figure 2 shows

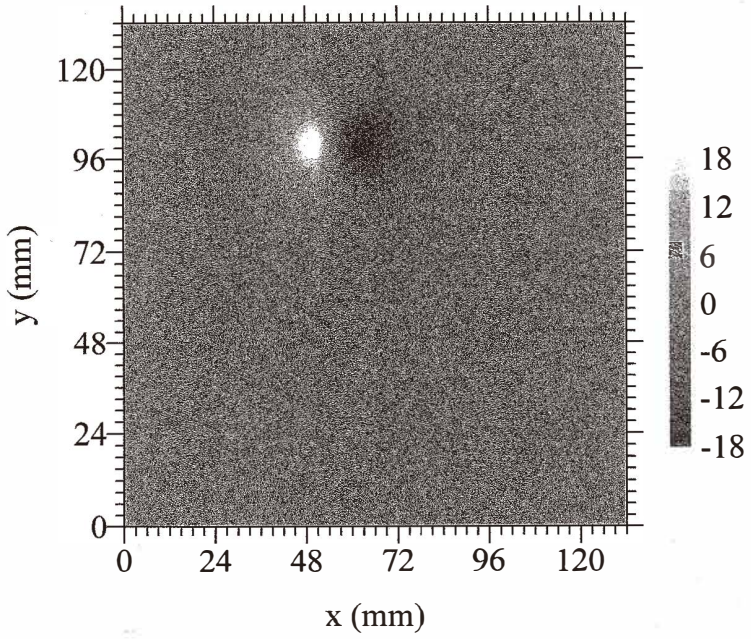

Fig. 2. Isofield map of the B_z component of the magnetic field for sample I (moment normal to the scanning direction). The dipole field is oriented perpendicular to the scanning direction. The scale is in nT.

a representative field map (B_z) of sample I with the magnetic moment normal to the scanning direction and the sample-to-sensor distance at 12 mm. The magnetic field is that of a dipole, positive at one side and negative at the other.

To estimate the field sensitivity of the sensors we scanned the pin sample. Figure 3 shows the magnetic field map for the pin (sample III) placed in vertical (the moment parallel to the z-axis, with a sensor-to-sample distance of 10 mm) and horizontal orientations. For the vertical case (Fig. 3(a)), it can be seen from the field map that the B_z component of the magnetic field exhibits axial symmetry as expected and the maximum magnetic field observed is around 10 nT. For the horizontal orientation (Fig. 3(b)) and with the sample 15 mm away from the sensors, the expected dipole field picture is obtained. The maximum measured field for the horizontal case was around 0.5 nT and the noise in the data was small. Some signal artifacts along the scanning direction due to the plexiglass arm are visible in this and other measurements. These artifacts degrade the field maps in Figs. 3(a) and 3(b) to some extent, but nevertheless the main features are clearly discernible.

The next step was to place the magnet samples I and II in different relative orientations and distances to determine the system's spatial resolution as a function of the separation and geometrical relationship of the individual samples. Figures 4(a) and 4(b) show the magnetic field map (B_z) when the two samples (I and II) are placed 25 mm apart, center-to-center distance, with the sensor-to-sample distances of 12 and 10 mm, respectively. For

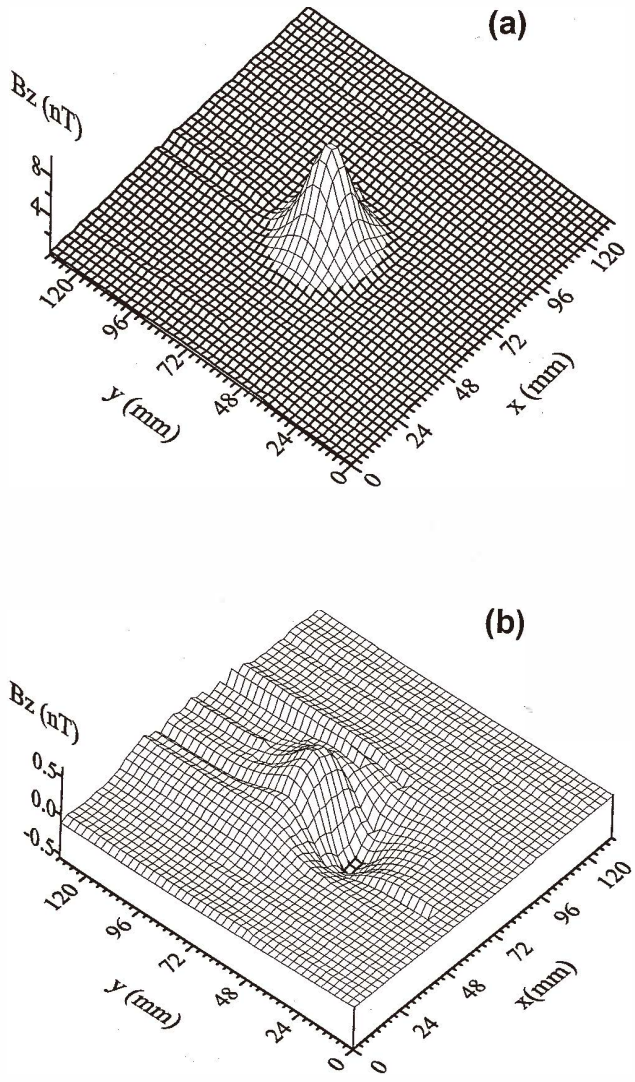

Fig. 3. Surface plot representation of the B_z component of the magnetic field for the pin (sample III) in both (a) vertical and (b) horizontal orientation. The scale is in nT.

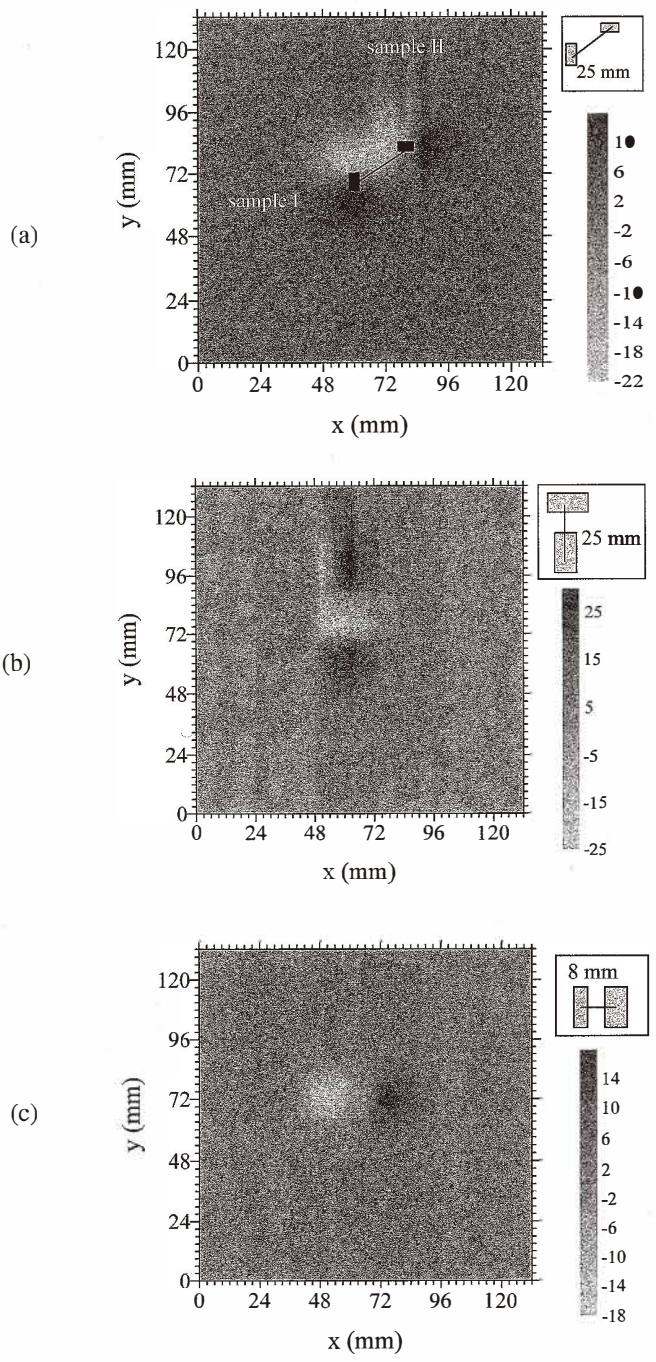

Fig. 4. Isofield maps of the B_z component of the magnetic field when the two samples (I and II) are placed as shown in the drawing at the upper left corner 25 mm apart ((a) and (b)) and 8 mm apart (c). The scale is in nT.

each case the overall field is the superposition of the magnetic fields produced by the individual samples, considered as dipoles. In Fig. 4(a) the axes of the samples are orthogonal, and this relative orientation is clearly seen in the field map. The center-to-center distance between the two samples can also be deduced accurately from the field map even though the sensor-to-sample distance is almost double the minimum attainable. In Fig. 4(b) the center of sample II lies along the axis of sample I. The relative orientation and center-to-center separation again can be deduced from the field map. Therefore, the spatial resolution even for relatively large sensor-to-sample distances is acceptable. In general, the spatial resolution of a mapping method that uses pickup coils of diameter d and a lift-off distance L is approximately equal to the larger of d or L. In our case the best spatial resolution is determined by the minimum stand-off distance and should be around 5–6 mm. The dimensions of the samples are difficult to determine from the data presented in Fig. 4, mainly because the relatively large stand-off distance combined with the 3 mm scanning step blurs their apparent size. A smaller step could improve the spatial resolution, but in this case the time needed for the measurement increases considerably.

Figure 4(c) shows the magnetic field map (B_z) when the two samples (I and II) are placed only 8 mm apart with a sensor-to-sample distance of 8 mm. The field map obtained resembles a large single dipole. This arises from the overlap of the magnetic fields of the two magnets.

Finally, we have also performed scans with an external magnetic field of 5 Oe at the sample using a system of compensating coils to null the field at the SQUIDs. The test samples were unglazed ceramic tiles with razor blade scratches 5 mm long. However, these initial tests were not successful as we observed a loss of lock for the SQUIDs. This is attributed to the small residual field (less than 1 Oe) at the SQUIDs which degraded their performance substantially. Work is underway to improve the system of compensating coils.

4. Discussion and Conclusions

In conclusion, we have tested an NDE system based on commercial high-T_c SQUID sensors and determined its sensitivity and spatial resolution under zero applied magnetic field inside a magnetic shield. The use of the shield was necessary for the SQUIDs to operate. We could measure signals of the order of 0.5 nT. The resolution of the system was adequate to give accurate field maps in two measurements when the samples were separated by 25 mm, even for relatively large sample-to-sensor stand-off distances. For smaller separations the magnetic fields produced by the samples overlap and the resolution of the system is adequate for measuring the resultant field distribution. Initial tests with ceramic samples under an externally applied magnetic field demonstrated the inadequacy of the SQUIDs in even small residual fields. Either better compensating circuitry and coil design or better SQUIDs are necessary. The finding that the SQUIDs could not operate properly without the magnetic shield certainly indicates that their quality must be improved.

Acknowledgments

This work was supported by the EKBAN-391 national project of the Greek Secretariat for Research and Technology of the Development of Ministry. We are also grateful to Dr. Harold Weinstock (United States Air Force Office for Scientific Research) for his continuous support and invaluable help.

References

1 H. Weinstock and M. Nisenoff: Review of Progress in QNDE **6** (1985) 660.
2 H. Weinstock and M. Nisenoff: SQUID '85, 3rd International Conference on Superconducting Quantum Devices, eds. H. D. Hahlbohm and H. Lubbig (deGruyter, Berlin, 1985) p. 843.
3 R. J. P. Bain, G. B. Donaldson, S. Evanson and G. Hayward: SQUID '85 – Superconducting Quantum Interference Devices and Their Applications, eds. H. D. Hahlbohm and H. Lubbig (deGruyter, Berlin, 1985) p. 841.
4 D. C. Hurley, Y. P. Ma, S. Tan and J. P. Wikswo Jr.: Review of Progress in Quantitative Nondestructive Evaluation, eds. D. O. Thompson and D. E. Chimenti (Plenum, New York, 1993) **12** 633.
5 D. C. Hurley, Y. P. Ma, S. Tan and J. P. Wikswo Jr.: Res. Nondestr. Eval. **5** (1993) 1.
6 J. P. Wikswo Jr., Y. P. Ma, N. G. Sepulveda, S. Tan, I. M. Thomas and A. Lauder: IEEE Trans. Appl. Supercond. **5** (1995) 1995.
7 W. G. Jenks, S. S. H. Sadeghi and J. P. Wikswo Jr.: J. Phys. D: Appl. Phys. **30** (1997) 293.
8 I. M. Thomas, Y. P. Ma, S. Tan and J. P. Wikswo Jr.: IEEE Trans. Appl. Supercond. **3** (1993) 1937.
9 D. S. Buchanan, D. B. Crum, D. Cox and J. P. Wikswo Jr.: Advances in Biomagnetism, eds. S. J. Williamson, M. Hoke, G. Stroink and M. Kotani (Plenum, New York, 1990) p. 677.
10 J. Z. Sun, W. J. Gallagher and R. H. Koch: Phys. Rev. B **50** (1994) 13664.
11 R. H. Koch, J. R. Rozen, J. Z. Sun and W. J. Gallagher: Appl. Phys. Lett. **63** (1993) 403.
12 R. H. Koch, J. Z. Sun, V. Foglietti and W. J. Gallagher: Appl. Phys. Lett. **67** (1995) 709.
13 Y. Tavrin, Y. Zhang, W. Wolf and A. I. Braginski: Supercond. Sci. Technol. **7** (1994) 265.
14 D. F. He, J.-H. Krause, Y. Zhang, M. Bick, H. Soltner, N. Wolters, W. Wolf and H. Bousack: to be published in IEEE Trans. Appl. Supercond.
15 J. P. Wikswo, Jr.: IEEE Trans. Appl. Supercond. **5** (1995) 74.
16 A. Cohran, J. C. Macfarlane, L. N. C. Morgan, J. Kuznik, R. Weston, L. Hao, R. M. Bowman and G. B. Donaldson: IEEE Trans. Appl. Supercond. **4** (1994) 128.
17 Y. Tavrin, H.-J. Crause, W. Wolf, V. Glyantsev, J. Schubert, W. Zander and H. Bousack: Cryogenics, **36** (1996) 83.
18 J. Clarke: SQUID Sensors: Fundamentals, Fabrication and Applications, ed. H. Weinstock (Kluwer, Dodrecht, 1996) pp. 1–62.
19 R. Hohmann, H.-J. Krause, H. Soltner, M. I. Faley, Y. Zhang, C. A. Kopetti, H. Bousack and A. I. Braginski: IEEE Trans. Appl. Supercond. **7** (1997) 2860–2865.
20 H. Weinstock, N. Tralshawala and J. R. Claycomb: to be published in IEEE Trans. Appl. Supercond.
21 I. M. Thomas, Y. P. Ma and J. P. Wikswo Jr.: IEEE Trans. Appl. Supercond. **3** (1993) 1949.
22 G. B. Donaldson, A. Cohran and D. McA. McKirdy: SQUID Sensors: Fundamentals, Fabrication and Applications, ed. H. Weinstock (Kluwer, Dodrecht, 1996) p. 599.
23 R. Cantor: SQUID Sensors: Fundamentals, Fabrication and Applications, ed. H. Weinstock (Kluwer, Dodrecht, 1996) p. 179.